Current Research in Food Science 3 (2020) 113–121

Contents lists available at ScienceDirect

Current Research in Food Science

journal homepage: www.editorialmanager.com/crfs/

Research Paper

# Structural characterization of nanoemulsions stabilized with sodium caseinate and of the hydrogels prepared from them by acid-induced gelation

Juan Manuel Montes de Oca-Avalos [a,1], Cristián Huck-Iriart [b], Virginia Borroni [a], Karina Dafne Martínez [a], Roberto Jorge Candal [c], María Lidia Herrera [a,*]

[a] Institute of Polymer Technology and Nanotechnology, University of Buenos Aires-CONICET, Facultad de Arquitectura, Diseño y Urbanismo, Intendente Güiraldes 2160, Pabellón III, C1428EGA, Ciudad Autónoma de Buenos Aires, Argentina
[b] Laboratorio de Cristalografía Aplicada, Escuela de Ciencia y Tecnología, Universidad Nacional de San Martín (UNSAM), Campus Miguelete, 25 de Mayo y Francia, 1650, San Martín, Provincia de Buenos Aires, Argentina
[c] Instituto de Investigación e Ingeniería Ambiental, Universidad Nacional de San Martín (UNSAM), Campus Miguelete, 25 de Mayo y Francia, 1650, San Martín, Provincia de Buenos Aires, Argentina

ARTICLE INFO

*Keywords:*
Nanostructure
SAXS
Guinier-porod model
Nanoemulsion
Hydrogel

ABSTRACT

Hydrogels obtained by acidification with glucono-δ-lactone (GDL), starting from nanoemulsions formulated with different concentrations of sodium caseinate (1–4 wt%) or 4 wt% sodium caseinate and sucrose (2–8 wt%), were prepared with the aim of quantifying structural parameters of both, initial nanoemulsions and hydrogels after 2.5 h of GDL addition, using the Guinier-Porod (GP) or the generalized GP models. Gelation process was followed by performing in situ temperature-controlled X-ray small angle scattering experiments (SAXS) using synchrotron radiation. In nanoemulsions, the calculated radius of gyration for oil nanodroplets ($Rg_{oil}$) decreased with increasing protein concentration and for the 4 wt% protein nanoemulsion, with increasing sucrose content. Calculated values of $Rg_{oil}$ were validated correlating them with experimental Z-average values as measured by dynamic light scattering (DLS). For hydrogels, radii of gyration for the sphere equivalent to the hydrogel scattering object ($R_{gsph}$) were close to 3 nm while correlation distances among building blocks ($R_{g2}$) were dependent on formulation. They increased with increasing contents of sodium caseinate and sucrose. $R_{g2}$ parameter linearly correlated with hydrogel strength ($G'_{\infty}$): a more connected nanostructure led to a stronger hydrogel.

## 1. Introduction

Milk can be considered to be a colloidal emulsion of casein particles, historically called micelles. The native casein micelles are composed of a complex of associated protein and calcium phosphate of about 200 nm. The protein fraction of the casein micelles, which represents ~93% of its dry mass, is composed of four individual sub-micelles, called αs1-, αs2-, β- and κ-casein (De Kruif et al., 2012). Sodium caseinate (NaCas) is a commercial milk product obtained by removing most of calcium phosphate. The final product contains disaggregated sub-micelles of approximately 10–12 nm. Owing to its high nutritional value, health benefits, and desirable functional properties such as emulsification, water and fat-binding, thickening and gelation, sodium caseinate is now extensively used as an ingredient in food products. Fermentation of milk is of importance during the processing of a number of dairy products such as yoghurt-like desserts (Myllärinen et al., 2007). This process can be mimicked by acidifying sodium caseinate-stabilized nanoemulsions with GDL. Acid gelation occurs as the pH slowly decreases.

A hydrogel may be defined as a nonfluid colloidal or three-dimensional hydrophilic polymeric network with the capacity of imbibing large amounts of water (Elsayed, 2019). Hydrogels may be from synthetic, semi-synthetic, or natural origins. Natural biopolymers are preferred because they are non-toxic and are friendly to the environment. Hydrogels have applications in numerous fields. In the food industry, they performed a variety of functions, including nutrient and flavor

* Corresponding author.
*E-mail addresses:* jmontesdeocaav@gmail.com (J.M. Montes de Oca-Avalos), chuck@unsam.edu.ar (C. Huck-Iriart), mvirborroni@gmail.com (V. Borroni), karinadafnem@yahoo.com.ar, lherrera@fi.uba.ar (K.D. Martínez), rjcandal@gmail.com (R.J. Candal), mlidiaherrera@gmail.com (M.L. Herrera).
[1] Permanent address: Center for the Development of Advanced Materials and Nanotechnology, Universidad Nacional de Ingenieria, Av. Túpac Amaru 210, Rimac, Lima, Perú.

https://doi.org/10.1016/j.crfs.2020.03.010

carriers (Guo et al., 2013; López-Hortas et al., 2019), calorie reduction (Chung et al., 2013), trans and saturated fat replacements in desserts (Montes de Oca-Ávalos et al., 2019), and oral delivery of lipophilic active ingredients (Zhang et al., 2015), among others. The structural properties of those hydrogels were closely related to their performance for an intended application.

Nanoemulsions are usually defined as a thermodynamically unstable colloidal dispersion consisting of two immiscible or partially miscible liquids, with one of the liquids being dispersed as small spherical droplets (discontinuous phase) in the other liquid (continuous phase), with radius sizes of droplets smaller than 100 nm (McClements, 2012). Nanoemulsions present several advantages over conventional emulsions due to the small droplets size they contain: high optical clarity, good physical stability against gravitational separation or droplet aggregation, and enhanced bioavailability of encapsulated substances (Montes de Oca-Ávalos et al., 2017). Films or hydrogels prepared from sodium caseinate-stabilized nanoemulsions showed advantages compared to the ones obtained from conventional systems. The enhancement in properties was explained by higher homogeneity in the structure, in terms of distribution of dispersed phase and absence of droplets aggregates as analyzed by confocal laser scanning microscopy (Montes de Oca-Ávalos et al., 2019; Montes-de-Oca-Ávalos et al., 2018). In nano-based sodium caseinate films, this homogeneity led to improved physical properties such as water vapor permeability and stability with respect to oil release (Montes-de-Oca-Ávalos et al., 2018), while in nano-based hydrogels, led to lower porosity as described by X-ray microtomography and improved rheological properties (Montes de Oca-Ávalos et al., 2019).

Small-Angle X-ray Scattering (SAXS) is a technique that has been increasingly used in the past ten years to describe food structure (Montes de Oca-Ávalos et al., 2019; Ramel et al., 2016; Huck-Iriart et al., 2016; Fasolin et al., 2018; Li et al., 2018; Muneer et al., 2018; Wang et al., 2019; Martins et al., 2019), to name a few. SAXS technique has the advantage over other very established methods such as microscopy approaches (data are collected on a focal plane) that the obtained results give averaged information on the samples, analyzed in bulk, evaluating the whole volume with statistical significance (Costa da Silva et al., 2015; Anitas, 2019). The high photon flux of the synchrotron source allows in situ characterization of hydrogel formation in a sample holder and as samples suffer no manipulation or treatment, structure is analyzed without disturbing the systems. Besides, turbid samples such as nanoemulsion-based hydrogels are successfully analyzed (Montes-de-Oca-Ávalos et al., 2018). SAXS is a technique by which nanoscale density differences in a sample can be quantified by analyzing the elastic scattering behavior of X-rays when travelling through it. SAXS has been used for characterizing nanoscale electron density correlations and/or the shape of nanoscopics objects with sizes up to ~100 nm. Quantifying structure in nanoscale is of great importance since it has been proved in several systems that structural characteristics correlated with macroscopic properties such as rheological behavior under small or large deformation (Ramel et al., 2016; Wang et al., 2019). Traditionally, small angle X-ray scattering (SAXS) data are characterized by the Guinier and Porod regions. The model used in this work for fitting SAXS data is an empirical model that allows describing scattering objects of different geometries, from spherical (the Guinier-Porod model) to nonspherical objects such as rods, platelets or lamellae (the generalized Guinier-Porod model), (Hammouda, 2010).

The aim of the present work was to quantify structural elements of sodium caseinate hydrogels prepared by acidification with GDL and of the nanoemulsions from which they were prepared. The Guinier-Porod and the generalized Guinier-Porod models were used to calculate radii of gyration and structural parameters. The calculated data were compared with data measured with experimental techniques based on different principles than those of SAXS.

## 2. Materials and methods

### 2.1. Materials

Sodium caseinate (NaCas), sucrose (S), glucono delta-lactone (GDL), and sodium azide were purchased from Sigma (Sigma–Aldrich, St. Louis, Mo., USA). Ethyl acetate was obtained from Sintorgan (Sintorgan S.A., Buenos Aires, Argentina). All reagents used were of analytical grade. No further purification was performed. Bidistilled water was used in all experiments (18 mΩ; Milli-Q Water System, Millipore Corporation, Billerica, MA, USA). The lipid phase selected was commercial sunflower seed oil (SFO) with the following fatty acids composition: palmitic (5.7 wt%), stearic (4.3 wt%), arachidic (1.6 wt%), behenic (1.1 wt%), oleic (82.6 wt %), and linoleic (3.9 wt%) acids.

### 2.2. Hydrogels preparation

Hydrogels were obtained by acidifying nanoemulsions with GDL. Nanoemulsions were prepared using a combination of a high-energy homogenization and evaporative ripening methods previously reported for whey protein-stabilized systems, with minor changes (Lee and McClements, 2010). For studying the effect of protein and sucrose concentrations, eight nanoemulsions were prepared. Solutions with concentrations of 1, 2, 3, or 4 wt% of NaCas in water were prepared. The 4 wt % NaCas-stabilized nanoemulsion may also contain S added to the aqueous phase in concentrations of 2, 4, 6, or 8 wt%. The lipid phase was a solution of 15 wt% SFO in ethyl acetate. In all nanoemulsions prepared, the ratio NaCas/SFO was kept constant at 0.6. Sodium azide was used in a percentage of 0.01 wt% to prevent microbial contamination. Nanoemulsions preparation method comprises three stages: the formation of a coarse emulsion (droplets in the microns), further homogenization to obtain a fine emulsion (droplets from 0.2 to 0.6 μm in diameter) and solvent evaporation to give nanoemulsions. In the first step, lipid and aqueous phases were mixed using an Ultra-Turrax (UT) T18 high-speed blender (S 18N-19G dispersing tool, IKA Labortechnik, Janke & Kunkel, GmbH & Co., Staufen, Germany), operated at 20,000 rpm for 1 min. Samples were kept in an ice bath (0 °C) during processing. The process was repeated three times. In the second step, the resultant coarse emulsions were further homogenized for 20 min using an ultrasonic liquid processing (US), VIBRA CELL, VC750 (power 750 W, frequency 20 kHz) model (Sonics & Materials, Inc., Newtown, CT, USA), with a 13-mm-diameter and 136-mm-length tip. The selected amplitude was 30%. The temperature of the sample-cell was controlled by means of an ice bath (0 °C) with a temperature cut down control of 20 ± 1 °C during ultrasound treatment. After ultrasound treatment, fine emulsions were obtained, but droplets were still in the conventional emulsions range. In the third step, the prepared fine emulsions were placed in a rotary evaporator Buchi model R 100 (Buchi, Postfach, Switzerland) connected to a vacuum pump and a recirculating chiller to eliminate ethyl acetate. The degree of ethyl acetate evaporation was determined by carrying out a mass balance of emulsions before and after solvent evaporation (Lee and McClements, 2010). The process was performed at 45 °C for 20 min. Then, the samples were cooled quiescently to room temperature (22.5 °C). The pHs of the SFO emulsions were 6.66 ± 0.05, close to 7. No buffer was added to the emulsions. Nanoemulsions were analyzed for droplet size distribution immediately after preparation. The average diameter of droplets (Z-average) was obtained from the distribution in volume using a DLS device NanoBrook 90Plus Particle Size Analyzer (Brookhaven Instruments Corporation, New York, USA), equipped with a laser and

operated at room temperature. Nanoemulsions were diluted in distilled water until the final concentration of NaCas was 0.1 wt%. The measurements were performed in duplicate with a scattering angle of 90°. For hydrogel formation, GDL was added to nanoemulsions at a GDL/NaCas ratio of 0.2. This GDL/NaCas ratio was chosen because it was the one that allowed obtaining the best rheological properties of all the ratios tested (Montes de Oca-Ávalos et al., 2019). The final pH value was 4.75 ± 0.20. The required amount of GDL was accurately weighed and added to 10 g of nanoemulsions. GDL was dissolved by stirring tubes with a vortex for 10 s and nanoemulsion was immediately placed in a SAXS cell for liquids previously described (Cavalcanti et al., 2004).

### 2.3. SAXS measurements

Small angle X-Ray scattering (SAXS) measurements were performed in the SAXS1 beamline of the Brasilian National Laboratory of Synchrotron Light (LNLS, Campinas, Brazil). For all experiments, the selected wavelength was 1.548 Å. A Pilatus 300K detector was used with a distance sample/detector of 3090.7 mm. The scattering intensity distributions as a function of scattering vector q were obtained in the q range between 0.035 and 1.33 $nm^{-1}$, with $q = (4\pi/\lambda)\sin(\theta) = 2\pi/d$, where λ is the radiation wavelength, 2θ is the scattering angle, and d is the interplanar distance. The SAXS patterns were recorded with exposure times of 1 min and a resting time of 1 min. Samples were analyzed for up to 2.5 h. Temperature in the liquid cell was controlled at 22.5 °C using a water bath. One-dimensional curves were obtained by integration of the 2D data using the program FIT-2D (Hammersley et al., 1996). The SAXS normalized patterns were fitted using the Guinier-Porod and the generalized Guinier-Porod model (Hammouda, 2010). Samples were analyzed by duplicate.

#### 2.3.1. Nanoemulsions characterization: the Guinier-Porod (GP) model

In nanoemulsion systems (initial state of gelation process), three objects contributed to the scattered intensity, $I(q)$: nanodroplets ($I_{oil}$), protein adsorbed on the interface ($I_{ads}$), and protein dispersed on the aqueous phase (free protein, $I_{free}$). The total intensity may be expressed as:

$$I(q) = I_{oil} + I_{ads} + I_{free} + back \quad (1)$$

where back is a constant background parameter.

To take into account the relative contribution of each scattering element, a scale factor (*SC*) was included:

$$I(q) = SC_{oil}P_{oil}(q) + SC_{ads}P_{ads}(q) + SC_{free}P_{free}(q) + back \quad (2)$$

with $P_{oil}$, $P_{ads}$, and $P_{free}$ the form factors of oil nanodroplets, adsorbed protein, and free protein, respectively.

To evaluate *P*, a Guinier–Porod empirical model developed by Hammouda was selected (Hammouda, 2010). The form factor is given by two contributions, the Guinier ($P_1$) and Porod ($P_2$) terms:

$$P_1(q) = \frac{1}{q_c^s}\exp\left(-\frac{q^2R_g^2}{3-s}\right) \quad \text{for } q \le q_c \quad (3)$$

$$P_2(q) = \frac{D}{q^d} \quad \text{for } q \ge q_c \quad (4)$$

where $R_g$ is the radius of gyration, *s* is a parameter related to object symmetry, *d* is the Porod exponent, and *D* is a scaling factor. Parameter *s* is equal to 0 for spherical objects, to 1 for rods or rigid cylinders, and to 2 for flat objects or lamellas. In addition, a Porod exponent of 4, points to particles with smooth surfaces while a value of 3, points to very rough surfaces (Guinier et al., 1955).

With the requirement that the values of the Guinier and Porod terms and their slopes (derivatives) be continuous at a value $q_c$, the following relationships are obtained:

$$q_c = \frac{[(d-s)(3-s)/2]^{1/2}}{R_g} \quad (5)$$

$$D = \exp\left(-\frac{q_c^2R_g^2}{3-s}\right)q_c^{d-s} \quad (6)$$

and therefore, including *D*, equations (3) and (4) may be written as follows:

$$P_1(q) = \frac{1}{q_c^s}\exp\left(-\frac{q^2R_g^2}{3-s}\right) \quad \text{for } q \le q_c \quad (7)$$

$$P_2(q) = \exp\left(-\frac{q_c^2R_g^2}{3-s}\right)\frac{q_c^{d-s}}{q^d} \quad \text{for } q \ge q_c \quad (8)$$

Due to the large oil/water interface area of nanoemulsions, free NaCas lose the casein-casein correlation, which is visible as a broad peak at intermediate angles (Huck-Iriart et al., 2016), in consequence, no structure factor was employed to interpret the systems studied in this work.

#### 2.3.2. Gels characterization: the generalized Guinier-Porod (GP) model

The model in 2.3.1 is not suitable for nonspherical scattering objects (Hammouda, 2010). To evaluate protein contribution in hydrogels, the selected model was the generalized Guinier-Porod approach, which is applicable for quantifying structures with scattering objects such as rods or lamellae (Luzzati, 1960; Hjelm et al., 1992; Hammouda, 2010). NaCas was the matrix in hydrogels, and therefore, adsorbed (molecules at the interface oil/water) and free (micelles dispersed in the aqueous phase) protein cannot be distinguished since molecules are connected to form a tridimensional network. In the case of hydrogels, equations (1) and (2) became:

$$I(q) = I_{oil} + I_{prot} + back \quad (9)$$

where $I_{prot}$ is the scattered intensity of total protein.

$$I(q) = SC_{oil}P_{oil}(q) + SC_{prot}P_{prot}(q) + back \quad (10)$$

As in the case of nanoemulsions, in hydrogels, the scattering parameters of nanodroplets were evaluated from $P_{oil}$ using the Guinier-Porod approach. Protein scattering objects were quantified from $I_{prot}$ using the generalized Guinier-Porod model, with the following equations:

$$P_1(q) = \frac{1}{q^{s_2}}\exp\left(-\frac{q^2R_{g2}^2}{3-s_2}\right) \quad q \le q_2 \quad (11)$$

$$P_2(q) = \frac{G}{q^{s_1}}\exp\left(-\frac{q^2R_{g1}^2}{3-s_1}\right) \quad q_2 \le q \le q_1 \quad (12)$$

$$P_3(q) = \frac{D}{q^d} \quad q \ge q_1 \quad (13)$$

where *G* and *D* are scaling factors, $S_1$ and $S_2$ are two slopes in the Guinier zone, and $R_{g1}$ and $R_{g2}$ are distances corresponding to the scattering object, with $R_{g1} < R_{g2}$. According to (Hammouda, 2010), "3 - $s_2$ and 3 - $s_1$ are the dimensionality parameters, and $R_{g2}$ and $R_{g1}$ are the radii of gyration for the short and overall sizes of the scattering object". In this work, interpretation of $R_{g2}$ parameter was the same as the cutoff distance for the fractal model (Huck-Iriart et al., 2016). This approach was previously reported by Pink et al. (2013) and Quinn et al., 2014. In those articles, parameters obtained from other X-ray techniques such as ultra-small X-ray scattering (USAXS) were also interpreted in a fractal way (Pink et al., 2013; Quinn et al., 2014). Considering that the global function and

their slopes (derivatives) must be continuous at $q_1$ and $q_2$, the following relationships are obtained:

$$q_2 = \left( \frac{s_1 - s_2}{\frac{2}{3-s_2}R_{g_2}^2 - \frac{2}{3-s_1}R_{g_1}^2} \right)^{1/2} \tag{14}$$

$$G = \exp\left[ - q_2^2 \left( \frac{R_{g_1}^2}{3-s_1} - \frac{R_{g_2}^2}{3-s_2} \right) \right] q_2^{(s_2 - s_1)} \tag{15}$$

$$q_1 = \frac{1}{R_{g_1}} \left[ (d - s_1) \frac{3 - s_1}{2} \right]^{1/2} \tag{16}$$

$$D = G \exp\left( - \frac{q_1^2 R_{g_1}^2}{3 - s_1} \right) q_1^{(d - s_1)} \tag{17}$$

Including these expressions in $P$, the generalized Guinier-Porod model may be written as follows:

$$P_1(q) = \frac{1}{q^{s_2}} exp\left( - \frac{q^2 R_{g_2}^2}{3 - s_2} \right) \qquad q \le q_2 \tag{18}$$

$$P_2(q) = \frac{q_2^{(s_2 - s_1)}}{q^{s_1}} \exp\left[ - \frac{q^2 R_{g_1}^2}{3 - s_1} - q_2^2 \left( \frac{R_{g_1}^2}{3 - s_1} - \frac{R_{g_2}^2}{3 - s_2} \right) \right] \qquad q_2 \le q \le q_1 \tag{19}$$

$$P_3(q) = \frac{G q_1^{(d - s_1)}}{q^d} \exp\left( - \frac{q_1^2 R_{g_1}^2}{3 - s_1} \right) \qquad q \ge q_1 \tag{20}$$

The values of $R_{g1}$ do not correspond to scattering objects with spherical symmetry. To compare the parameters calculated for hydrogels with that calculated for nanoemulsions, radius of gyration of the sphere equivalent to the hydrogel scattering object ($R_{gsph}$) were obtained with the following equation:

$$R_{gsph} = \frac{2\sqrt{3} R_{g1}}{[(4 - s_1)(3 - s_1)]^{1/2}} \tag{21}$$

The Guinier-Porod model allows calculating droplet coverage ($C$), that is total surface occupied by adsorbed protein, by the limit in the Porod region as follows (Guinier et al., 1955):

$$C \propto \frac{SC_{ads} \left[ P_{GP}^{ads}(q)\, q^4 \right] q \to \infty}{\Delta \rho_{ads}^2} \tag{22}$$

where, $\Delta\rho_{ads}$ is the difference in electronic density between adsorbed protein and the background. Protein density was set at 1,1 × $10^{-5}$ Å$^2$, taken into account literature values, and density change due to sucrose addition was considered as reported (Perriman et al., 2008). Replacing the expression for Porod region in Ec. 22, and considering that $d = 4$ and $s = 0$, it becomes:

$$C \propto \frac{SC_{ads}}{\Delta \rho_{ads}^2} \frac{36\, e^2}{R_g^4} \tag{23}$$

### 2.4. Rheological measurements

Gelation under shear was followed by dynamic oscillatory rheology using a Paar PhysicaMCR 300 rheometer (Anton Paar Inc., Ashland, USA). After adding GDL, approximately 1.2 g of emulsion was immediately loaded into parallel plates (PP30/S) separated by 1 mm and changes in $G'$ and $G''$ moduli with time were monitored. Data were taken at 22.5 °C, every 2 min, and were recorded for up to 3 h. Studies were performed with a 0.01% strain at a constant frequency of 1 Hz. Asymptotic values of $G'$ ($G'_\infty$) were calculated from $G'$ vs. time curves using values of time higher than the time at which $G' = G''$, with the following empirical equation:

$$logG' = logG'_\infty \left[ \frac{k_1 t}{1 + k_1 t} \right] \tag{24}$$

where $k_1$ is a constant and $t$ is the time. Values of $G'_\infty$ are the average of three determinations.

### 2.5. Statistical analysis

For the SAXS model, the parameter "$R$ value" was selected to provide an indicator of the fit quality (Breβler et al., 2015). It was calculated using the following equation:

$$R\ value = \frac{\sum_{i=1}^{N} \left| |I_{exp}(q_i)| - |I_{mod}(q_i)| \right|}{\sum_{i=1}^{N} |I_{exp}\ (q_i)|} \tag{25}$$

A $R$ value ranging between 0 and about 0.1 indicates a good to acceptable fit, whereas large values (up to infinity) denote a poor fit.

## 3. Results

### 3.1. Quantification of nanoemulsions structure

#### 3.1.1. SAXS data

Fig. 1 shows the results obtained when all nanoemulsions were analyzed by SAXS. As may be observed, for all q values, total intensity increased with increasing concentrations of protein. In a previous work, Z-average of these nanoemulsions was reported to decrease with increasing NaCas concentrations (Montes de Oca-Ávalos et al., 2017). In other words, the percentage of droplets in the nano range (not invisible for SAXS technique) increased for the 4 wt% NaCas nanoemulsions compared to the 1 wt% NaCas system. Changes in total intensities were in agreement with these findings. The number of scattering objects with sizes within SAXS measurements range (~100 nm) increased and therefore intensity was the highest for the more concentrated formulation (4 wt% NaCas nanoemulsion). The increase in sucrose concentration led to an increase in intensity only in the low q values, showing a different behavior than for protein concentration. The effect of sucrose on total intensity could be expected to involve other mechanisms of action (see below results and discussion sections).

#### 3.1.2. Nanoemulsions fitted by GP model

Table 1 reports the values of Guinier-Porod model parameters selected for fitting nanoemulsions SAXS curves. All scattering objects, oil droplets, protein micelles (free in bulk), and protein adsorbed at the interface were considered spherical, and therefore, parameter $s$ was set at 0. All surfaces were considered smooth with parameter $d$ equal to 4. Values of calculated parameters corresponded to average values of scattering objects. A lower limit of 15 nm for $R_g$ values of oil droplets was selected taken into account previous DLS results (Montes de Oca-Ávalos et al., 2017). Radius of protein objects adsorbed at the interface was considered 3 nm as previously reported (Huck-Iriart et al., 2016).

As an example, Fig. 2 shows the results of fitting the 4NaCas0S-nanoemulsion SAXS curve with the GP model. The experimental data, the calculated total intensity, and the contributions of the three scattering objects (nanodroplets, adsorbed protein, and free protein) are reported. The sum of the three contributions fitted experimental values very well as may be observed from values of parameters $R$ (Table 2). As expected,

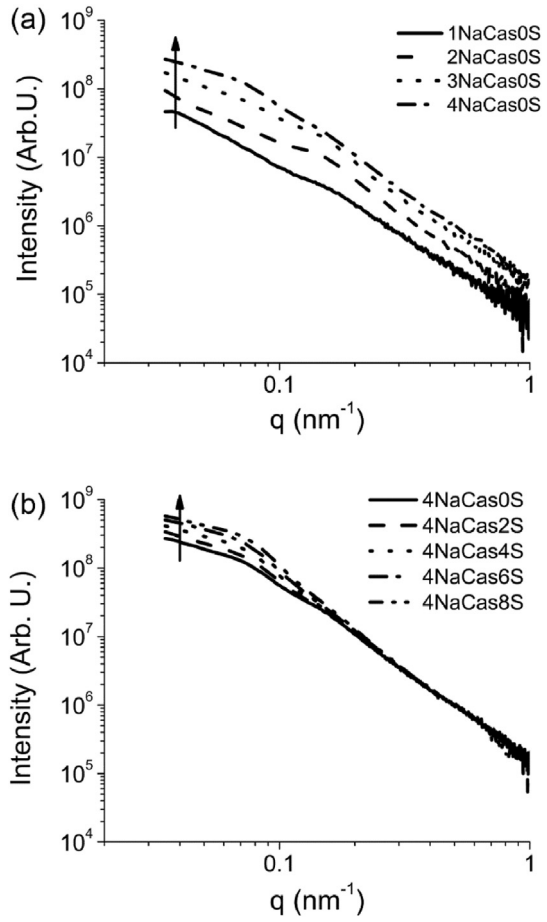


**Fig. 1.** Normalized scattered intensity (Arb.U.) as a function of scattering vector q (nm$^{-1}$) for nanoemulsions prepared with a) 1, 2, 3 or 4 wt% NaCas without sucrose and b) 4 wt% NaCas with 0, 2, 4, 6, or 8 wt% sucrose.

**Table 1**
Values of Guinier Porod model parameters selected for fitting nanoemulsions small angle x-ray scattering (SAXS) curves.

| | Oil nanodroplets (oil) | Adsorbed Protein (ads) | Free Protein (free) |
|---|---|---|---|
| Scaling Factor | Free | Free | Free |
| $R_g$ | Free (>15 nm) | Fix at 3 nm | Free |
| d | Fix at 4 (smooth surface) | Fix at 4 | Fix at 4 |
| s | Fix at 0 (sphere) | Fix at 0 | Fix at 0 |

from the analysis of all curves (see supplementary materials), $I_{oil}$ increased with increasing protein and sucrose contents since nanodroplets number also increased in both cases (lower z-average for higher protein and sucrose contents). $I_{ads}$ and $I_{free}$ increased when NaCas concentrations increased from 1 to 4 wt%. However, addition of sucrose to the 4 wt% NaCas nanoemulsion diminished both protein-intensities, indicating that protein/sucrose interactions were strong and able to modify protein/protein interactions.

The calculated radii of gyration for oil nanodroplets ($Rg_{oil}$) and free protein ($Rg_{free}$) are reported in Table 2. $Rg_{free}$ slightly increased with increasing protein concentration up to 4 wt% NaCas, while $Rg_{oil}$ always decreased; for the 4 wt% NaCas nanoemulsion $Rg_{free}$ significantly diminished. When protein content was 4 wt%, both radii diminished with increasing sucrose concentration. Taken into account that sphere radius ($R_S$) and $Rg$ are related by $R_S = \sqrt{\frac{5}{3}} R_g$ (Ramel et al., 2016), since each system presented a given size distribution, $R_s$ is a weighted average

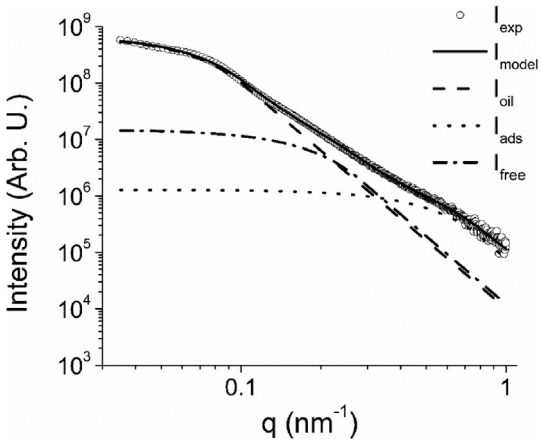


**Fig. 2.** Results of fitting the 4NaCas0S-nanoemulsion SAXS curve with the Guinier-Porod (GP) model. The plot shows experimental data ($I_{exp}$), global fit of the model ($I_{model}$), and the contribution of the three scattering objects considered: oil nanodroplets ($I_{oil}$), adsorbed protein ($I_{ads}$) and free protein ($I_{free}$).

**Table 2**
Gyration radii for oil nanodroplets ($Rg_{oil}$) and free protein ($Rg_{free}$) for all nanoemulsions.

| Sample | Protein | Oil nanodroplets | Goodness of fit |
|---|---|---|---|
| | $Rg_{free}$ (nm) | $Rg_{oil}$ (nm) | R |
| 1NaCas0S | 10.18 ± 0.05$^a$ | 36.0 ± 0.2$^a$ | 0.041 |
| 2NaCas0S | 10.65 ± 0.05$^b$ | 35.0 ± 0.2$^b$ | 0.053 |
| 3NaCas0S | 11.74 ± 0.05$^c$ | 32.6 ± 0.02$^c$ | 0.037 |
| 4NaCas0S | 10.74 ± 0.05$^d$ | 26.44 ± 0.09$^d$ | 0.026 |
| 4NaCas2S | 10.33 ± 0.05$^e$ | 25.63 ± 0.02$^e$ | 0.027 |
| 4NaCas4S | 9.7 ± 0.2$^f$ | 24.84 ± 0.02$^f$ | 0.026 |
| 4NaCas6S | 9.0 ± 0.1$^g$ | 24.80 ± 0.02$^g$ | 0.021 |
| 4NaCas8S | 8.8 ± 0.2$^g$ | 23.9 ± 0.06$^h$ | 0.031 |

± Error of calculated parameter.

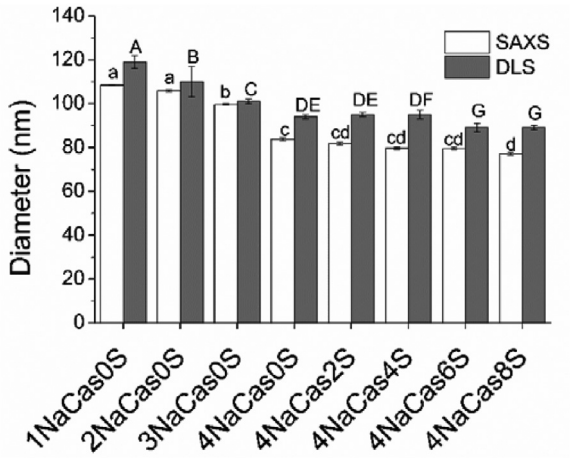


**Fig. 3.** Diameters obtained by fitting small angle X-ray scattering (SAXS) data with the Guinier-Porod (GP) model, (empty bars), and diameters measured by dynamic light scattering (DLS Z-average), (grey bars), for nanodroplets present in the emulsions studied. Different letters among each data set indicates significant differences ($p<0.05$).

radius (larger particles scatter X-ray more than small ones), the radius of a sphere composed of a nanodroplet covered by a layer of spherical protein particles, and therefore the diameter of droplet/covering scattering element, may be calculated. Fig. 3 reports the diameters calculated by fitting SAXS data with the GP model and the diameters (Z-average)

obtained by measuring droplets size distribution using DLS for all emulsions studied. As may be observed calculated values were always smaller than values measured by DLS. However, tendencies were similar: values significantly diminished with increasing concentrations of protein, and for the same protein concentration, with increasing sucrose concentrations ($p < 0.05$). Although significant, differences due to the addition of sucrose were smaller than the ones obtained increasing NaCas concentration. It was expected that DLS values were greater than values calculated from SAXS curves. DLS measures not only droplets/coverage size but also hydration layer that moves with nanodroplet. In addition to *R* values (Table 2), the fact that values from two different techniques correlated indicated that SAXS model assumptions regarding geometry and particle surface were correct.

### 3.1.3. Droplet coverage

Fig. 4 reports droplet coverage (*C*), as total surface occupied by adsorbed protein, for all samples. *C* significantly increased with increasing protein content ($p 7< 0.05$). *C* value for the 1 wt% NaCas-stabilized nanoemulsion was 4 times smaller than *C* value for the 4 wt % nanoemulsion since there is a higher concentration of total protein in the nanoemulsion and a higher dispersed oil concentration that must be coated to be stabilized. Thus, the molecules preferred to be located at the interface than to remain in solution forming micelles. On the other side, it might be expected that sucrose did not have an effect on droplet coverage since it is not a surfactant. However, for the 4 wt% NaCas-stabilized nanoemulsion, *C* slightly increased with increasing sucrose content: 2% coverage for every 2% increase in sucrose concentration. Sucrose slightly increased the tendency of being at the interface most likely because it interacted with protein molecules modifying protein/protein interactions and protein molecules affinity for the interface.

## 3.2. Quantification of nanogels structure

### 3.2.1. Gelation kinetics

Fig. 5 shows, as an example, gelation kinetics of the nanoemulsion formulated with 4 wt% NaCas and 8 wt% S. SAXS patterns reported were obtained every 20 min. As time passed, the intensity in the Guinier zone diminished (lower inset) while in the Porod zone increased (upper inset), indicating that there were structural changes confirming the occurrence of sol/gel transition. Changes in patterns indicated that the size of

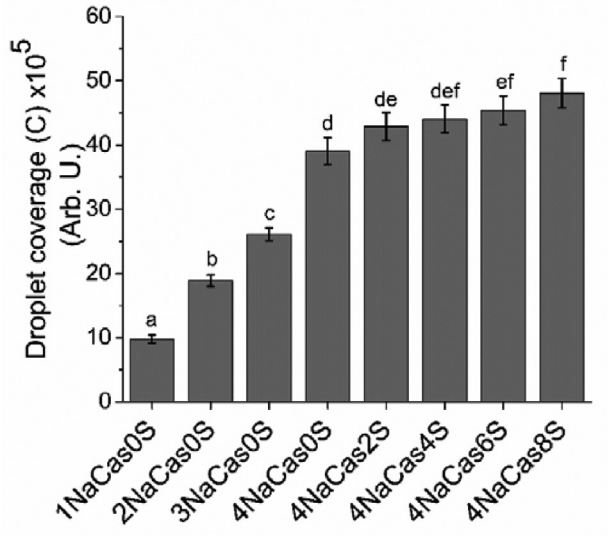


**Fig. 4.** Total area occupied by the adsorbed protein (C, in arbitrary units), calculated from the Porod zone. Different letters indicates significant differences ($p<0.05$).

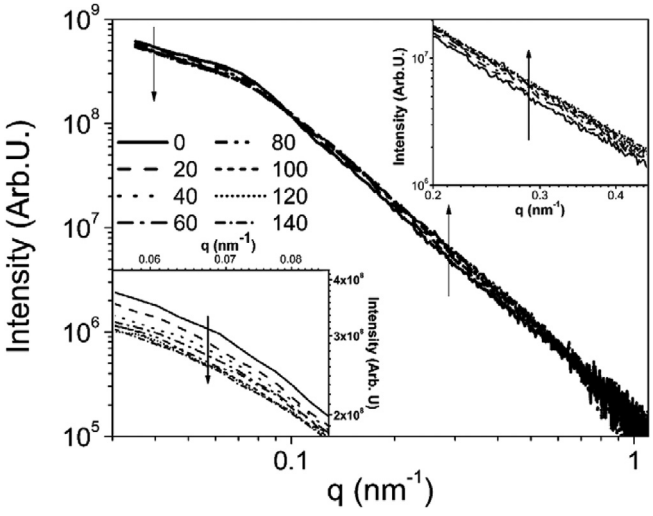


**Fig. 5.** Scattered intensity obtained every 20 min after glucone-δ-lactone (GDL) addition to the nanoemulsion with 4 wt% sodium caseinate (NaCas) and 8 wt% Sucrose, (GDL/NaCas ratio = 0.2). Lower inset: zoom of the Guinier zone. Upper inset: zoom of the Porod zone.

scattering elements and connections of matrix building blocks changed as the gelation progressed. These changes in the structure were very complicate and therefore only initial and final states were characterized.

### 3.2.2. Structural characterization of gels

SAXS curves for gels measured after 2.5 h of GDL addition were fitted by the GP model for nanodroplets and the generalized GP model for protein matrix. Table 3 summarizes the selected values for the models parameters. For oil nanodroplets, as was done when fitting nanoemulsions SAXS curves, *s* was set at 0 (sphere) and *d* at 4 (smooth surface). For protein scattering elements, $s_2$ was set at 0 since the Guinier region was successfully fitted using only one slope, and $s_1$ value was fitted by the program. In all cases, results were very close and therefore a fixed value of 2.6, which was the average value calculated for all SAXS curves, was selected for parameter $s_1$. As the radius of gyration of the sphere equivalent to the hydrogel scattering object ($R_{gsph}$) depends on $s_1$ and $Rg_1$, by fixing $s_1$, $R_{gsph}$ only depended on $Rg_1$. Distances $Rg_1$ and $Rg_2$ varied freely and were fitted by the program because the behavior during sol/gel transition was not known and therefore these values were hard to predict. $Rg_1$ corresponded to the size of the scattering object, which was not spherical since protein formed a network and no isolate protein objects can be identified in this matrix. $Rg_2$ was related to the length of interactions among building blocks and it might be expected that the higher the $Rg_2$ value the stronger the gel.

Fig. 6 reports the intensity vs. q curve for the hydrogel prepared from the 4NaCas8S nanoemulsion. Fig. 6 shows experimental data ($I_{exp}$), global fit of the model ($I_{model}$), and the contributions of the two scattering elements considered: oil nanodroplets ($I_{oil}$) and protein ($I_{prot}$). The calculated intensity fitted the experimental data very well. Parameter *R* also confirmed the goodness of the fit (Table 4). For all samples, both

**Table 3**
Values of the GP and the generalized GP models parameters selected for fitting nanogels SAXS data.

| | Oil nanodroplets (GP) | Protein (Generalized GP) |
|---|---|---|
| Scale Factor | Free | Free |
| Gyration radius | $R_g$ Free (>15 nm) | $Rg_1$ and $Rg_2$ free |
| d | Fix at 4 (smooth surface) | Fix at 4 |
| s | Fix at 0 (sphere) | $s_2$ fix at 0 |
| | | $s_1$ fix at 2.6 |

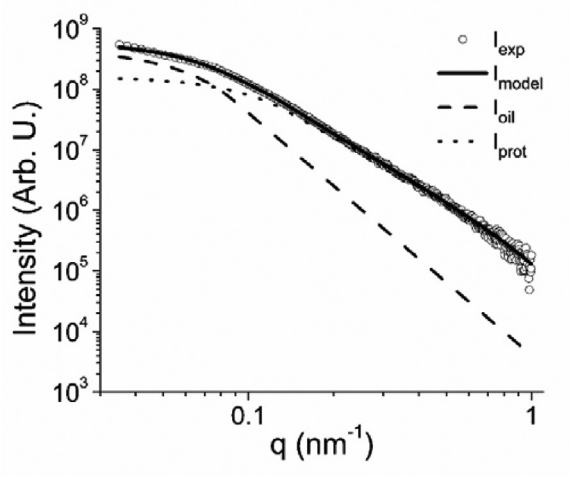


**Fig. 6.** Results of fitting small angle X-ray (SAXS) data with the generalized Guinier-Porod (GP) model for the 4 wt% sodium caseinate (NaCas) 8 wt% sucrose nano-based hydrogel. The plot shows experimental data ($I_{exp}$), global fit of the model ($I_{model}$), and the contribution of the two scattering elements considered: oil nanodroplets ($I_{oil}$) and protein ($I_{prot}$).

contributions, $I_{oil}$ and $I_{prot}$ increased with increasing contents of protein and sucrose, indicating that more scattering elements were present in hydrogels containing a higher solid mass (see supplementary materials). Table 4 reports values of parameters obtained from the GP model for nanodroplets, from the generalized GP model for protein scattering objects, and values of radius of gyration of the sphere equivalent to the hydrogel scattering object ($R_{gsph}$). As mentioned before, $Rg_1$ and $Rg_2$ may be interpreted as radius of gyration for building blocks and correlation length between building blocks, respectively. $Rg_1$ slightly increased with increasing protein concentration and for the 4 wt% NaCas hydrogel, no significant differences were found with increasing sucrose concentration, indicating that building blocks were similar for different formulations ($p < 0.05$). $Rg_2$ significantly increased with increasing protein concentration and for a fixed protein content, slightly increased with increasing sucrose content. Connections among building blocks were improved for hydrogels containing a higher solid mass. Radius of gyration of oil nanodroplets ($R_{goil}$) significantly diminished with increasing protein and sucrose concentrations. According to these calculations, nanodroplets kept their original nanosize, which slightly increased from nanoemulsion to gel. These results showed that droplet coalescence was negligible during the sol/gel transition and that scattering objects of hydrogel had nanosizes.

### 3.3. Sol/gel transition by rheology

Fig. 7 reports the evolution of $G'$ and $G''$ moduli as a function of time for the nanoemulsion/hydrogel transition. The starting nanoemulsion selected as example was the one formulated with 4 wt% NaCas and 8 wt % sucrose. At the beginning of the run, the behavior of $G'$ and $G''$ with time was characteristic of a liquid system. $G'$ and $G''$ values varied around zero. As the hydrogel formed, both moduli increased sharply. There is a time at which $G'$ is equal to $G''$ and after this point, $G'$ is always significantly higher than $G''$. There is a general agreement among authors considering gelation time as the time at which both moduli have the same value. After that time hydrogel was structured until reached a plateau value for $G'$ and $G''$. As was reported the degree of stiffness of gels may be inferred from asymptotic values of $G'$ ($G'_\infty$), (Raak et al., 2019). Fig. 8 shows a plot of log $G'_\infty$ vs. log $R_{g2}$. As may be noticed both parameters correlated. Longer distances of interactions among building blocks corresponded to greater gel strength. The hydrogel prepared from the 4 wt% NaCas/8 wt% sucrose nanoemulsion was not included in Fig. 8 because for this sample there was a notorious increase in $G'_\infty$, greater than the one expected from the linear tendency showed for the other formulations. This hydrogel had the greatest strength of all systems studied and the highest solid mass of all. In this formulation, in addition to building blocks connections, solid mass also contributed to rheology.

## 4. Discussion

Previous work on sodium caseinate/trehalose conventional emulsions showed that the protein-to-oil ratio modified droplets size of discontinuous phase and strongly influences stability and destabilization mechanisms (Cerimedo et al., 2010). In this article, the protein-to-oil ratio was fixed at 0.6. However, for the prepared nanoemulsions, Z-average and polydispersity index as measured by DLS decreased while stability as evaluated by Turbiscan notoriously increased (de Oca-Ávalos et al., 2017), indicating that droplets size and stability depended on more than one parameter. Other factors such as total solid mass were also important since they affected droplet coverage ($C$), influencing the affinity of protein molecules for the interface, and also the interactions among protein molecules, as may be inferred from parameter $C$. This increase in droplet coverage was in agreement with the fact that radius of gyration of free protein ($Rg_{free}$) significantly diminished for the 4 wt% NaCas-stabilized nanoemulsion while droplets size notoriously decreased, indicating that more protein was at the interface and less molecules interacted in solution to form micelles. As previously reported this formulation was stable for 2 months (Cerimedo et al., 2010). The effects of total solid mass were also noticeable in the nanoemulsion-based hydrogels as evidenced by the behavior of parameters $R_{g2}$ and $G'_\infty$. The highest the solid mass the greater the correlation distances and final strength of hydrogels.

Increasing sucrose content had a lower effect on systems parameters than increasing protein concentration. However, sucrose modified interactions among protein molecules increasing parameter C, and decreasing $Rg_{free}$ and $Rg_{oil}$ values. In conventional systems, addition of 20 wt% sucrose to a 5 wt% NaCas emulsion modified the long-term adsorption of NaCas at oil/water interface, and significantly changed interfacial dynamic characteristics, indicating that because of sucrose addition, NaCas became a better surfactant. In those systems, the interactions between sucrose and NaCas modified protein functionality,

**Table 4**
Gyration radii for oil nanodroplets (Rg) and protein ($Rg_2$ and $Rg_1$) as well as the radius of the equivalent sphere for all nanogels.

| Sample | Protein | | | Oil Nanodroplets | Goodness of fit |
|---|---|---|---|---|---|
| | $Rg_2$ (nm) | $Rg_1$ (nm) | $Rg_{sph}$ (nm) | Rg (nm) | R |
| N1NaCas0S | 7.11 ± 0.05$^a$ | 0.30 ± 0.002$^a$ | 1.80 ± 0.01$^a$ | 43.57 ± 0.3$^a$ | 0.061 |
| N2NaCas0S | 8.88 ± 0.06$^b$ | 0.43 ± 0.003$^b$ | 2.56 ± 0.02$^b$ | 42.88 ± 0.3$^b$ | 0.039 |
| N3NaCas0S | 11.68 ± 0.08$^c$ | 0.42 ± 0.003$^b$ | 2.50 ± 0.02$^b$ | 48.74 ± 0.4$^c$ | 0.018 |
| N4NaCas0S | 13.03 ± 0.09$^d$ | 0.56 ± 0.004$^c$ | 3.33 ± 0.02$^c$ | 46.90 ± 0.3$^d$ | 0.014 |
| N4NaCas2S | 13.44 ± 0.09$^e$ | 0.55 ± 0.003$^c$ | 3.28 ± 0.02$^c$ | 39.99 ± 0.3$^e$ | 0.019 |
| N4NaCas4S | 14.18 ± 0.1$^f$ | 0.55 ± 0.003$^c$ | 3.31 ± 0.02$^c$ | 33.45 ± 0.2$^f$ | 0.026 |
| N4NaCas6S | 14.56 ± 0.1$^g$ | 0.60 ± 0.004$^c$ | 3.56 ± 0.03$^c$ | 32.38 ± 0.2$^g$ | 0.027 |
| N4NaCas8S | 14.64 ± 0.1$^g$ | 0.52 ± 0.003$^c$ | 3.11 ± 0.02$^d$ | 27.34 ± 0.2$^h$ | 0.030 |

± Error of calculated parameter.

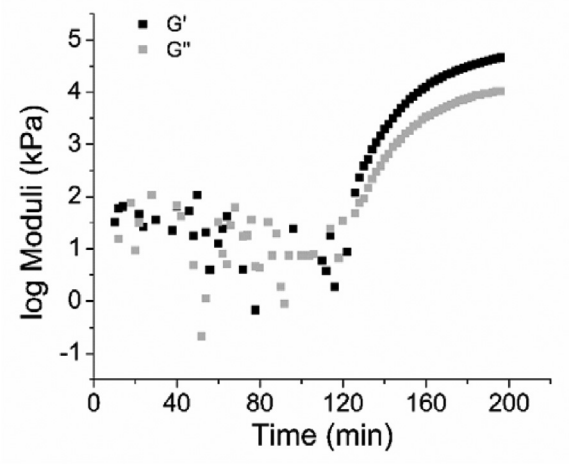


**Fig. 7.** Elastic (G′) and loss (G″) moduli as a function of gelation time for the nanoemulsion formulated with 4 wt% sodium caseinate (NaCas) and 8 wt% sucrose. Black symbols: G′, grey symbols G''.

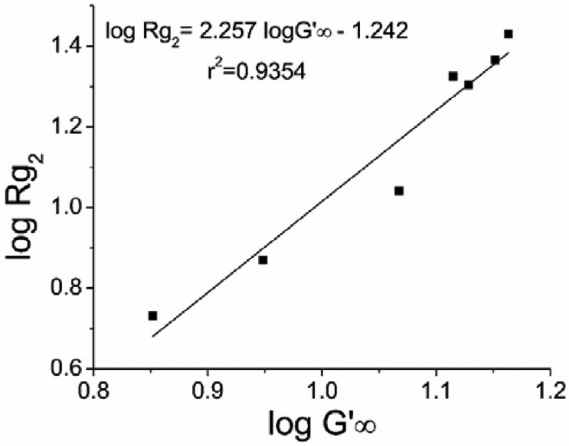


**Fig. 8.** Plot of log $G'_{\infty}$ vs log $R_{g2}$. Data were linearly fit, equation and $R^2$ are shown in the graph.

which led to a dramatic change in emulsion microstructure and stability (Huck-Iriart et al., 2013). SAXS calculated parameters supported this effect on nanosystems too. However, as stability of nanoemulsions is notoriously higher than the one of conventional emulsions with the same formulations, it occurred in less extent. Microtomography analysis of hydrogels prepared from nanoemulsions showed that porosity decreased and wall thickness increased with increasing sucrose content (Montes de Oca-Ávalos et al., 2019). Sucrose was part of hydrogel structure, indicating that protein/sucrose interactions are strong and that these interactions modified the affinity among protein molecules. These findings are in agreement with the fact that $R_{g2}$ distance increased with increasing sucrose concentration, indicating interactions among a higher number of building blocks. Rheological parameter $G'_{\infty}$ showed good correlation with $R_{g2}$ distance as reported in Fig. 8. A more connected nanostructure led to a stronger hydrogel.

The curve $I_{prot}$ vs. q was also fitted using a fractal approach (see supplementary materials). The fractal dimension obtained was 2.5, a value very close to $s_1$ value, a Guinier slope in the medium zone of I vs. q curve, showing that all nano-based hydrogels had the same symmetry for connections between building blocks. The linear correlation between $R_{g2}$ and $G'_{\infty}$ reported in Fig. 8 confirmed that all hydrogels were fractal in nature. The calculated slope was 2.3, a value close to the fractal dimension calculated by the fractal model. The correlation distances calculated from the fractal model were in agreement with $R_{g2}$ distances, which supported the physical interpretation chosen for parameter $R_{g2}$.

## 5. Conclusions

Hammouda approach (Hammouda, 2010) was successfully used to interpret nano-based sodium caseinate/sucrose hydrogels and the nanoemulsions that were used to prepare them.

In hydrogels, two different types of objects were described together: oil droplets and protein building blocks. These objects had different geometries, however, they were quantified from a curve that described the whole q range. The model had the advantage of allowing protein building blocks quantification without assigning a geometry to them. Guinier zone was fitted with only one slope with low error, which indicated that all analyzed hydrogels had the same symmetry for building blocks connections. In both, nanoemulsions and nano-based hydrogels, model parameters correlated with macroscopic physical properties: calculated values of radius of gyration of nanodroplets ($Rg_{oil}$) showed the same tendencies as Z-average values measured by DLS, and long distances, assigned to connections between building blocks, ($Rg_2$), correlated with $G'_{\infty}$ values, indicating that the connections between building blocks (nano scale) strongly influenced hydrogel strength (macroscopic system).

## CRediT authorship contribution statement

**Juan Manuel Montes de Oca-Avalos:** Data curation. **Cristián Huck-Iriart:** Software, Data curation. **Virginia Borroni:** Formal analysis, Writing - original draft. **Karina Dafne Martínez:** Writing - original draft. **Roberto Jorge Candal:** Conceptualization, Methodology. **María Lidia Herrera:** Conceptualization, Methodology, Writing - original draft.

## Declaration of Competing Interest

None.

## Acknowledgments

This work was supported by the University of Buenos Aires [grant number 20020170100039BA]; the Synchrotron Light National Laboratory (LNLS), Campinas, Brazil [grant numbers D11A-SAXS1-14296, SAXS1-20150056]; and the Argentinian National Agency for the Promotion of Science and Technology (ANPCyT) [grant number PICT 2018-00868].

## Appendix A. Supplementary data

Supplementary data to this article can be found online at https://doi.org/10.1016/j.crfs.2020.03.010.

## References

Anitas, E.M., 2019. Small-angle scattering from weakly correlated nanoscale mass fractal aggregates. Nanomaterials 9 (4), 648. https://doi.org/10.3390/nano9040648.

Breßler, I., Kohlbrecher, J., Thünemann, A.F., 2015. SASfit: a tool for small-angle scattering data analysis using a library of analytical expressions. J. Appl. Crystallogr. 48 (5), 1587–1598. https://doi.org/10.1107/S1600576715016544.

Cavalcanti, L.P., Torriani, I.L., Plivelic, T.S., Oliveira, C.L.P., Kellermann, G., Neuenschwander, R., 2004. Two new sealed sample cells for small angle x-ray scattering from macromolecules in solution and complex fluids using synchrotron radiation. Rev. Sci. Instrum. 75 (11), 4541–4546. https://doi.org/10.1063/1.1804956.

Cerimedo, M.S.Á., Iriart, C.H., Candal, R.J., Herrera, M.L., 2010. Stability of emulsions formulated with high concentrations of sodium caseinate and trehalose. Food Res. Int. 43 (5), 1482–1493. https://doi.org/10.1016/j.foodres.2010.04.008.

Chung, C., Degner, B., Decker, E.A., McClements, D.J., 2013. Oil-filled hydrogel particles for reduced-fat food applications: fabrication, characterization, and properties. Innovat. Food Sci. Emerg. Technol. 20, 324–334. https://doi.org/10.1016/j.ifset.2013.08.006.

Costa da Silva, D., Huck-Iriart, C., Kellermann, G., Giovanetti, L.J., Craievich, A.F., Requejo, F.G., 2015. In situ study of the endotaxial growth of hexagonal CoSi2 nanoplatelets in Si (001). Appl. Phys. Lett. 107 (22), 223101. https://doi.org/10.1063/1.4936377.

De Kruif, C.G., Huppertz, T., Urban, V.S., Petukhov, A.V., 2012. Casein micelles and their internal structure. Adv. Colloid Interface Sci. 171, 36–52. https://doi.org/10.1016/j.jcis.2012.01.002.

de Oca-Ávalos, J.M., Candal, R.J., Herrera, M.L., 2017. Colloidal properties of sodium caseinate-stabilized nanoemulsions prepared by a combination of a high-energy homogenization and evaporative ripening methods. Food Res. Int. 100, 143–150. https://doi.org/10.1016/j.foodres.2017.06.035.

Elsayed, M.M., 2019. Hydrogel preparation technologies: relevance kinetics, thermodynamics and scaling up aspects. J. Polym. Environ. 27 (4), 871–891. https://doi.org/10.1007/s10924-019-01376-4.

Fasolin, L.H., Cerqueira, M.A., Pastrana, L.M., Vicente, A.A., Cunha, R.L., 2018. Thermodynamic, rheological and structural properties of edible oils structured with LMOGs: influence of gelator and oil phase. Food Struct. 16, 50–58. https://doi.org/10.1016/j.foostr.2018.03.003.

Guinier, A., Fournet, G., Yudowitch, K.L., 1955. In Small-Angle Scattering of X-Rays. John Wiley and Sons, New York, p. 268. https://doi.org/10.1002/pol.1956.120199326.

Guo, J., Jin, Y.C., Yang, X.Q., Yu, S.J., Yin, S.W., Qi, J.R., 2013. Computed microtomography and mechanical property analysis of soy protein porous hydrogel prepared by homogenizing and microbial transglutaminase cross-linking. Food Hydrocolloids 31 (2), 220–226. https://doi.org/10.1016/j.foodhyd.2012.10.023.

Hammersley, A.P., Svensson, S.O., Hanfland, M., Fitch, A.N., Hausermann, D., 1996. Two-dimensional detector software: from real detector to idealised image or two-theta scan. Int. J. High Pres. Res. 14 (4–6), 235–248. https://doi.org/10.1080/08957959608201408.

Hammouda, B., 2010. A new Guinier–Porod model. J. Appl. Crystallogr. 43 (4), 716–719. https://doi.org/10.1107/S0021889810015773.

Hjelm Jr., R.P., Thiyagarajan, P., Alkan-Onyuksel, H., 1992. Organization of phosphatidylcholine and bile salt in rodlike mixed micelles. J. Phys. Chem. 96 (21), 8653–8661. https://doi.org/10.1021/j100200a080.

Huck-Iriart, C., Ruiz-Henestrosa, V.M.P., Candal, R.J., Herrera, M.L., 2013. Effect of aqueous phase composition on stability of sodium caseinate/sunflower oil emulsions. Food Bioprocess Technol. 6 (9), 2406–2418.

Huck-Iriart, C., Montes-de-Oca-Ávalos, J., Herrera, M.L., Candal, R.J., Pinto-de-Oliveira, C.L., Linares-Torriani, I., 2016. New insights about flocculation process in sodium caseinate-stabilized emulsions. Food Res. Int. 89, 338–346.

Lee, S.J., McClements, D.J., 2010. Fabrication of protein-stabilized nanoemulsions using a combined homogenization and amphiphilic solvent dissolution/evaporation approach. Food Hydrocolloids 24 (6–7), 560–569. https://doi.org/10.1016/j.foodhyd.2010.02.002.

Li, Z., Yang, Z., Otter, D., Rehm, C., Li, N., Zhou, P., Hemar, Y., 2018. Rheological and structural properties of coagulated milks reconstituted in D2O: comparison between rennet and a tamarillo enzyme (tamarillin). Food Hydrocolloids 79, 170–178. https://doi.org/10.1016/j.foodhyd.2017.12.004.

López-Hortas, L., Conde, E., Falqué, E., Domínguez, H., Torres, M.D., 2019. Preparation of hydrogels composed of bioactive compounds from aqueous phase of artichoke obtained by MHG technique. Food Bioprocess Technol. 1–12. https://doi.org/10.1007/s11947-019-02301-2.

Luzzati, V., 1960. Interprétation des mesures absolues de diffusion centrale des rayons X en collimation ponctuelle ou linéaire: solutions de particles globulaires et de batonnets. Acta Crystallogr. 13 (11), 939–945. https://doi.org/10.1107/S0365110X60002284.

Martins, A.J., Cerqueira, M.A., Pastrana, L.M., Cunha, R.L., Vicente, A.A., 2019. Sterol-based oleogels' characterization envisioning food applications. J. Sci. Food Agric. 99 (7), 3318–3325. https://doi.org/10.1002/jsfa.9546.

McClements, D.J., 2012. Edible delivery systems for nutraceuticals: designing functional foods for improved health. Ther. Deliv. 3 (7), 801–803. https://doi.org/10.4155/tde.12.56.

Montes de Oca-Ávalos, J.M., Candal, R.J., Herrera, M.L., 2017. Nanoemulsions: stability and physical properties. Curr. Opin. Food Sci. 16, 1–6. https://doi.org/10.1016/j.cofs.2017.06.003.

Montes de Oca-Ávalos, J.M., Borroni, V., Huck-Iriart, C., Navarro, A.S., Candal, R.J., Herrera, M.L., 2019. Relationship between formulation, gelation kinetics, micro/nanostructure and rheological properties of sodium caseinate nanoemulsion-based acid gels for food applications. Food Bioprocess Technol. 13 (2020), 288–299. https://doi.org/10.1007/s11947-019-02394-9.

Montes-de-Oca-Ávalos, J.M., Altamura, D., Candal, R.J., Scattarella, F., Siliqi, D., Giannini, C., Herrera, M.L., 2018. Relationship between nano/micro structure and physical properties of TiO2-sodium caseinate composite films. Food Res. Int. 105, 129–139. https://doi.org/10.1016/j.foodres.2017.11.011.

Muneer, F., Johansson, E., Hedenqvist, M.S., Plivelic, T.S., Markedal, K.E., Petersen, I.L., Kuktaite, R., 2018. The impact of newly produced protein and dietary fiber rich fractions of yellow pea (Pisum sativum L.) on the structure and mechanical properties of pasta-like sheets. Food Res. Int. 106, 607–618. https://doi.org/10.1016/j.foodres.2018.01.020.

Myllärinen, P., Buchert, J., Autio, K., 2007. Effect of transglutaminase on rheological properties and microstructure of chemically acidified sodium caseinate gels. Int. Dairy J. 17 (7), 800–807. https://doi.org/10.1016/j.idairyj.2005.10.031.

Perriman, A.W., McGillivray, D.J., White, J.W., 2008. Reactions of isolated monomolecular protein films. Soft Matter 4 (11), 2192–2198. https://doi.org/10.1039/B804711A.

Pink, D.A., Quinn, B., Peyronel, F., Marangoni, A.G., 2013. Edible oil structures at low and intermediate concentrations. I. Modeling, computer simulation, and predictions for X ray scattering. J. Appl. Phys. 114 (23), 234901. https://doi.org/10.1063/1.4847996.

Quinn, B., Peyronel, F., Gordon, T., Marangoni, A., Hanna, C.B., Pink, D.A., 2014. Aggregation in complex triacylglycerol oils: coarse-grained models, nanophase separation, and predicted x-ray intensities. J. Phys. Condens. Matter 26 (46), 464108. https://doi.org/10.1088/0953-8984/26/46/464108.

Raak, N., Schöne, C., Rohm, H., Jaros, D., 2019. Acid-induced gelation of enzymatically cross-linked caseinate in different ionic milieus. Food Hydrocolloids 86, 43–49. https://doi.org/10.1016/j.foodhyd.2018.01.037.

Ramel Jr., P.R.R., Peyronel, F., Marangoni, A.G., 2016. Characterization of the nanoscale structure of milk fat. Food Chem. 203, 224–230. https://doi.org/10.1016/j.foodchem.2016.02.064.

Wang, Y., Eastwood, B., Yang, Z., de Campo, L., Knott, R., Prosser, C., Hemar, Y., 2019. Rheological and structural characterization of acidified skim milks and infant formulae made from cow and goat milk. Food Hydrocolloids 96, 161–170. https://doi.org/10.1016/j.foodhyd.2019.05.020.

Zhang, Z., Zhang, R., Tong, Q., Decker, E.A., McClements, D.J., 2015. Food-grade filled hydrogels for oral delivery of lipophilic active ingredients: temperature-triggered release microgels. Food Res. Int. 69, 274–280. https://doi.org/10.1016/j.foodres.2015.01.004.